ENVIRONMENTAL RESEARCH
LETTERS

PURPOSE-LED PUBLISHING™
Celebrating the 20th anniversary of Environmental Research Letters

LETTER • **OPEN ACCESS**

Attribution and projection of February extreme rainfall events in Southeast Africa

To cite this article: Donghyun Lee *et al* 2026 *Environ. Res. Lett.* **21** 184038

View the article online for updates and enhancements.

You may also like

- Reducing nitrate loads to the St. Lawrence river could mitigate hypoxia and acidification in its deep estuary and Gulf
David Lévesque, Diane Lavoie, Aude Boivin-Rioux et al.
- Simulating microplastic distribution in oceans: the impact of morphology and sources
Anne Gaymard, Camille Richon, Matthias Egger et al.
- Implementing just fossil fuel transition: extreme Citizen Science to enforce the ban on gas flaring activities in the Ecuadorian Amazon
Francesco Facchinelli, Alberta Pavone, Edoardo Crescini et al.

This content was downloaded from IP address 165.120.83.41 on 22/10/2026 at 14:34

ENVIRONMENTAL RESEARCH
LETTERS

Check for updates

OPEN ACCESS

RECEIVED
22 June 2026

REVISED
1 September 2026

ACCEPTED FOR PUBLICATION
15 September 2026

PUBLISHED
25 September 2026

Original content from this work may be used under the terms of the Creative Commons Attribution 4.0 licence.

Any further distribution of this work must maintain attribution to the author(s) and the title of the work, journal citation and DOI.

LETTER

Attribution and projection of February extreme rainfall events in Southeast Africa

Donghyun Lee[1,*], **Carol Chen**[1], **Paulo Ceppi**[1], **Friederike Otto**[2], **In-Hong Park**[3], **Nicholas Leach**[4], **Sarah Sparrow**[5] **and Myles Allen**[4,6]

[1] Department of Physics, Imperial College London, London, United Kingdom
[2] The Grantham Institute for Climate Change, Imperial College London, London, United Kingdom
[3] Department of Civil and Environmental Engineering, Konkuk University, Seoul 05029, Republic of Korea
[4] Atmospheric Ocean and Planetary Physics, University of Oxford, Oxford, United Kingdom
[5] Department of Engineering, Oxford E-Research Centre, University of Oxford, Oxford, United Kingdom
[6] School of Geography and Environment, University of Oxford, Oxford, United Kingdom
[*] Author to whom any correspondence should be addressed.

E-mail: donghyun.lee@imperial.ac.uk

Keywords: extreme precipitation, extreme event attribution, extreme event projection, generalized extreme value distribution, risk assessment, Mozambique, Zimbabwe, Southeast Africa

Supplementary material for this article is available online

Abstract

Record-breaking extreme rainfall events, such as those observed in Southeast Africa (SEAF) in February 2023, underscore the urgent need to quantify anthropogenic impacts on extreme weather risks. This study presents an attribution and projection analysis of February extreme rainfall in SEAF by evaluating probabilistic risk changes across multiple Earth System Model (ESM) ensembles and numerical weather prediction (NWP) experiments. While NWP models reliably capture the magnitude and frequency of these extremes, ESMs generally exhibit a wet bias, necessitating the use of relative thresholds. Our attribution analysis reveals that greenhouse gas (GHG) forcing significantly increases the risk of extreme events (e.g. once-in-70-year and once-in-150-year events, comparable to the precipitation intensities of 2000 and 2023). However, this risk increase remains less certain under all-forcing simulations, as ESMs show substantial disagreement regarding aerosol (AER) influences. Future projections under various shared socioeconomic pathways indicate that a higher GHG emission exacerbates these risks, highlighting the critical importance of aggressive mitigation efforts. Furthermore, shifts in generalized extreme value (GEV) parameters demonstrate how forcing-driven climate changes may deform the risk probability distribution, with a higher emission of GHG potentially altering both the climatological mean and interannual variability of SEAF extreme rainfall. Our findings are supported by both ESM and NWP results (particularly short-lead forecasts), with the latter exhibiting lower uncertainty due to constraints on synoptic systems and internal oceanic variability. We conclude that GHG forcing likely elevates the risk of 2023-like extreme events in SEAF and discuss the remaining sources of uncertainty in these projections.

1. Introduction

During the austral summer, Southeast Africa (SEAF) is highly susceptible to extreme rainfall peaking in February, primarily driven by the South Indian Ocean Convergence Zone (Fučkar *et al* 2020). In 2023, the Mascarene High intensified this inland moisture transport, interacting with cut-off lows (Fazel-Rastgar *et al* 2025) and steering tropical cyclones toward landfall (Serele *et al* 2023). These extremes inflict disproportionate social-economic damage (Banda and Bangidza 2025, Nganhane *et al* 2025) and trigger health crises (Aderinto 2023, Braka *et al* 2024), while ensuing landslides severely threaten food and water security (Taylor *et al* 2013, Serele *et al* 2023).

With the increasing frequency of these events, extreme event attribution (EEA) has gained

© 2026 The Author(s). Published by IOP Publishing Ltd

significant attention over the past two decades (Allen 2003, Perkins-Kirkpatrick *et al* 2022). A primary objective in this field is to determine whether anthropogenic forcings have modified the characteristics of such extremes. Previous studies have utilized the trend-fitting probabilistic approach (TPA) to investigate SEAF extreme rainfall, often focusing on the global warming level (GWL) as a key driver of changes in probability distributions (Fučkar *et al* 2020, Philip *et al* 2020, Otto *et al* 2022, Pinto *et al* 2026). While TPA provides rapid statistical assessments, observational TPA results often conflict with numerical simulations under factual-like forcings.

This inconsistency arises largely from the sensitivity of linear trends between GWL and extreme events (Fučkar *et al* 2020, Otto *et al* 2022, Pinto *et al* 2026). Since extreme events involve a complex interplay of weather noise, natural variability, and combined forcings such as greenhouse gases (GHG), aerosols (AER) and natural drivers (NAT) like volcanic and solar activity (Haustein *et al* 2016, Min 2020, Kim *et al* 2024, Lee *et al* 2024, Takahashi *et al* 2025), the inherent statistical limitations of TPA often lead to an underestimation of risk (Nordling *et al* 2025, Takahashi *et al* 2025).

An alternative EEA framework is the modeled probabilistic approach (MPA), which contrasts Earth System Model (ESM) simulations under factual and counterfactual conditions (Gillett *et al* 2016). Large ensembles of ESMs allow for the quantification of linear and non-linear impacts of isolated anthropogenic forcing (GHG & AER), and NAT (Dong *et al* 2021, Wang *et al* 2023, Kim *et al* 2024). However, model diversity in representing ocean states, parameterization, and weather noise often introduces considerable uncertainty.

To mitigate this, recent studies have adopted the 'storyline approach,' which constrains uncertainty at the process level (Shepherd *et al* 2018). This method employs ESMs with dynamical nudging (e.g. Wehrli *et al* 2020, Van Garderen *et al* 2021) or free-running numerical weather prediction (NWP) models under perturbed atmospheric or oceanic conditions (e.g. Leach *et al* 2021, 2024). By constraining the synoptic development of target extreme events, the storyline approach, and its probabilistic variant, the storyline-based probabilistic approach (SPA), significantly reduces uncertainty compared to traditional MPA (Lee *et al* 2024, Barriopedro *et al* 2025, León-FonFay *et al* 2026).

Despite these advancements, SEAF extreme rainfall has yet to be comprehensively examined using both MPA and SPA frameworks. To resolve previous uncertainties, this study combines ESM-based MPA and NWP-based SPA to evaluate historical attribution and future projection risks under global warming scenarios, addressing two core questions: (1) Why do models often yield ambiguous attribution results compared to observational TPA? and (2) How will extreme rainfall risks evolve under different global warming mitigation pathways?

2. Data and methods

2.1. Observations

This study defines extreme rainfall as the maximum daily total precipitation occurring in February (Rx1d; Sillmann *et al* 2013) over the SEAF region (20° S – 28° S, 29° E – 36° E). To evaluate these events, we utilize the HadEX3 dataset (Dunn *et al* 2024) and derive Rx1d indices from daily precipitation datasets including the European Centre for Medium-Range Weather Forecasts (ECMWF) Reanalysis v5 (ERA5; Hersbach *et al* 2020), the gauge-based Global Precipitation Climatology Centre (GPCC; Becker *et al* 2013), and the Global Precipitation Climatology Project version 3.3 (GPCP3; Huffman *et al* 2023). We primarily rely on ERA5 for our analysis (e.g. Kim *et al* 2020) because reanalysis products provide superior spatio-temporal coverage compared to observational datasets, which may suffer from spatial inhomogeneity in station records or inconsistencies in satellite instrumentation and sensor calibration. Detailed descriptions of each dataset are provided in supplementary table 1.

2.2. ESM simulations

We use daily total precipitation data from ESMs participating in the Coupled Model Intercomparison Project Phase 6 (CMIP6), which provides standardized climate simulations from numerous international modeling centers (Eyring *et al* 2016). To attribute risk changes to specific forcings, we selected 13 ESMs that provide ensembles for factual historical simulations (ALL forcing) and counterfactual single-forcing experiments (GHG, AER, and NAT).

To project future risk, we utilize the same 13 ESMs that also include projections under three shared socioeconomic pathways (SSPs; Riahi *et al* 2017): SSP1-2.6 (sustainable development), SSP2-4.5 (middle-of-the-road scenario), and SSP5-8.5 (fossil-fuel-dependent development). Detailed information regarding the selected ESMs, CMIP6 experiments, and their respective ensemble members is provided in supplementary table 2.

2.3. NWP

To quantify risks through the SPA, we employ the ECMWF Integrated Forecasting System (IFS) CY47R3b (Forbes *et al* 2021). This system has been validated in recent EEA studies for its ability to simulate extreme events under controlled forcing conditions (Leach *et al* 2021, 2024, Ermis *et al* 2024, Lee *et al* 2024). The IFS is a coupled model incorporating atmospheric (Resolution: TCo639 ∼18 km with 137 vertical levels), wave (0.25°), sea ice (0.25°), and oceanic processes (ORCA025Z75 0.25° with 75

vertical levels), and generates 51-member ensembles through initial condition perturbation used in operational forecast (ECMWF 2021). We use daily precipitation datasets at 0.25° resolution interpolated by ECMWF MIR library (Malardel *et al* 2016).

We conducted three sets of NWP experiments by perturbing CO_2 concentrations and ocean states (sea ice, salinity, and 3D temperature) to reflect different climate conditions. The initial atmospheric, land, and oceanic states were sourced from the operational IFS.

- **NWP-ALL**: CO_2 at ∼420 ppm (current operational level).
- **NWP-PIC**: CO_2 at ∼285 ppm (pre-industrial levels) with anthropogenic impacts removed from ocean states.
- **NWP-FUT**: CO_2 at ∼615 ppm (representing future radiative forcing) with estimated anthropogenic impacts added to ocean states.

While the ensemble perturbations and atmospheric/-land initial conditions are identically paired across the NWP experiments, the paired oceanic initial states for NWP-PIC and NWP-FUT are modified with their respective anomalies.

Essentially, NWP-PIC represents pre-industrial conditions, while NWP-FUT is calibrated to be comparable to the SSP2-4.5 scenario. Unlike CMIP6 experiments, these NWP experiments treat non-CO_2 forcings (e.g. AER and non-CO_2 GHG) as invariant, allowing for a focused assessment of CO_2-driven impacts on extreme weather. Further details regarding experimental design are provided in Leach *et al* (2024).

To construct a 28 d period representing February 2023 for each lead-time group, we concatenated 4 d forecast windows from seven initialization dates chosen from a 9-date pool, varying by lead time (supplementary table 3): short (S; 3–6 d), medium (M; 7–10 d), and long (L; 11–14 d). Our major NWP conclusions rely on the NWP-S group, with NWP-M and NWP-L serving as sensitivity tests. Additionally, operational forecasts initialized on February 1st, 11th, and 21st (1985–2023) were used to establish the NWP climatology (1985–2014) and evaluate performance (supplementary figure 1).

2.4. Generalized extreme value (GEV) distributions

To quantify extreme event probabilities, we employ a stationary GEV distribution. Notably, we first compute Rx1d on native grids (supplementary table 1 and 2), and then calculate their regionally weighted average as the SEAF February extreme event (details in supplementary Text 1). L-moments are used for parameter estimation, as they offer robustness even with limited sample sizes (e.g. Kharin *et al* 2007, Min *et al* 2009, Kim *et al* 2020, Leach *et al* 2021, Lee *et al* 2024). The probability of an extreme rainfall event exceeding a magnitude x is given by:

$$P(x) = 1 - \mathrm{F}(x;\mu,\sigma,\xi) \tag{1}$$

where $F\ (x;\ \mu,\ \sigma,\ \xi)$ is the cumulative distribution function of the GEV, defined as:

$$\mathrm{F}(x;\mu,\sigma,\xi) = \begin{cases} \exp\left[-\exp\left\{-\frac{x-\mu}{\sigma}\right\}\right], \xi = 0 \\ \exp\left[-\left\{1+\xi\frac{x-\mu}{\sigma}\right\}^{-\xi^{-1}}\right], \xi \neq 0, 1+\xi\frac{x-\mu}{\sigma} > 0 \end{cases} \tag{2}$$

The GEV parameters—location (μ), scale (σ), and shape (ξ)—represent the mean, dispersion, and type of distribution (Gumbel, Fréchet, or Weibull types) of the extreme rainfall distribution, respectively. We use 30 years February to compute climatological GEV of present (1985–2014) and future (2071–2100) for each ESM. For NWP, we use 51 ensembles to compute GEV for February 2023 at different CO_2 and ocean conditions. To account for estimation uncertainty, we apply a bootstrapping process (Davison and Hinkley 1997) to generate 100 000 bootstrap resamples per model. Multi-model assessments use an equally-weighted pooled mixture of 1300 000 resamples. Supplementary Text 1 details these methods, including independent resampling.

We interpret forcing-driven changes by comparing shifts in μ, σ, and ξ (Kodra and Ganguly 2014), consistent with the nonstationary GEV framework (Abdelmoaty and Papalexiou 2023, Jayaweera *et al* 2025). Furthermore, we quantify the relative change in risk probability using the risk ratio (RR, equation (3) where C1 and C2 indicate samples from different forcing conditions (e.g. Fučkar *et al* 2020, Leach *et al* 2021, Kim *et al* 2024, Lee *et al* 2024). For attribution, we use ALL, GHG, AER or NWP-ALL for C1 and NAT or NWP-PIC for C2 to show attribution of extreme events to human-induced forcings, and SSP1-2.6, SSP2-4.5, SSP5-8.5 or NWP-FUT for C1 and ALL or NWP-ALL for C2 to show projected changes of extreme events to different warming scenarios at the end of 21st Century:

$$RR(C1/C2)_X = P(X)_{C1}/P(X)_{C2}. \tag{3}$$

Following IPCC guidance (Mastrandrea *et al* 2011, Kause *et al* 2022), we evaluate the statistical significance of RR, classifying results as 'extremely likely' (>95% probability) or 'likely' (>66% probability).

3. Results

3.1. February extreme rainfall events in SEAF

The observed characteristics of Rx1d and their statistically derived risk probabilities for record-shattering events are illustrated in figure 1. The

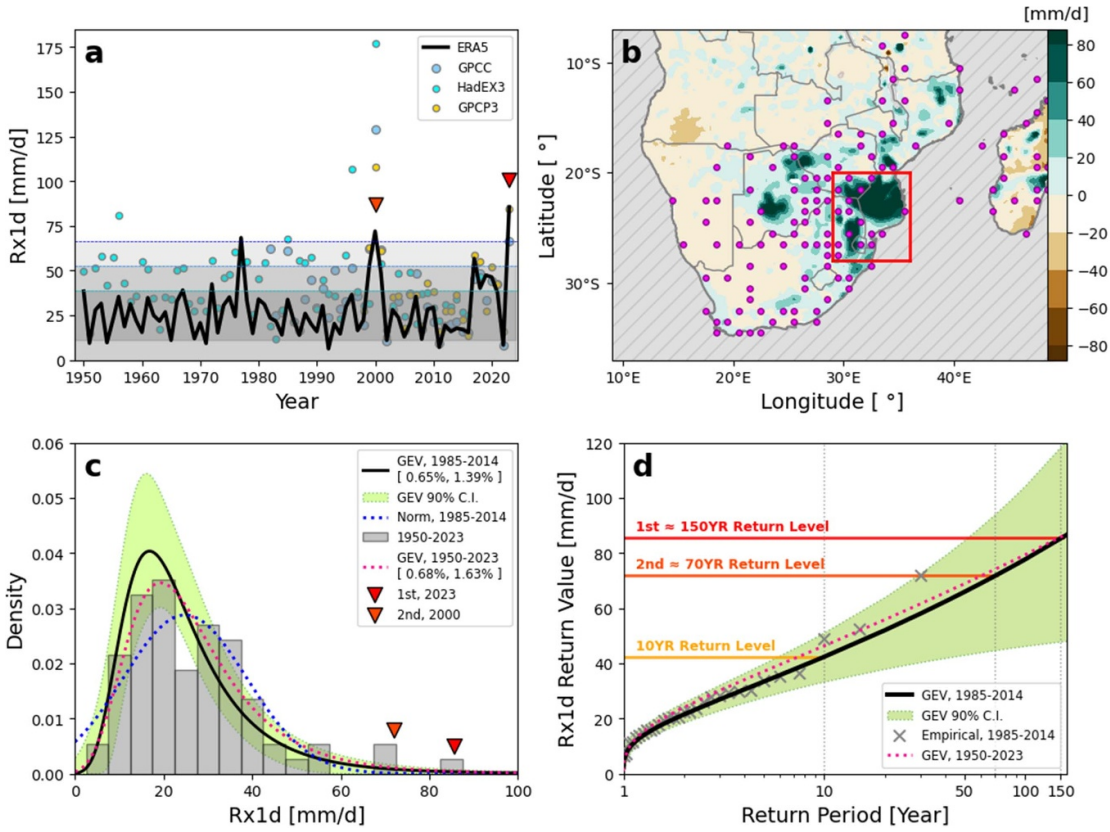


Figure 1. (a) Time series of February Rx1d over SEAF from ERA5 (line) and station-based observations (colored dots). The shaded background regions and dashed horizontal lines indicate one, two, and three standard deviations from the 1985–2014 climatological mean, and inverted red triangles mark the two highest events. (b) Spatial pattern of the February 2023 Rx1d anomaly. Dots indicate observation stations, and the red box defines the SEAF study region. (c) Probability distributions of February Rx1d for raw data (bars), normal distribution (blue dots), and GEV fits. Bracketed numbers indicate exceedance probabilities for the two extreme cases. The 90% confidence interval (green shading) is derived from 100 000 bootstrap resamples of the base period. (d) Return level plot comparing empirical data (crosses) and GEV fits. Vertical dotted lines highlight the target 10-year, 70-year (2000 event), and 150-year (2023 event) return periods.

74 year ERA5 Rx1d time series reveals three events exceeding three standard deviations above the climatological mean (figure 1(a)), two of which have occurred within the last 24 years. Despite the inherent spatio-temporal limitations of station-based observations, Rx1d values across all datasets consistently identify the events in 2000 and 2023 as highly anomalous.

The spatial pattern of the 2023 Rx1d anomaly highlights the characteristic nature of SEAF extreme rainfall (figure 1(b)), with the most severe precipitation occurring over southern Mozambique and Zimbabwe regions where operational station density is sparse. The 2000 and 2023 extreme events share a common pattern: anomalous dryness along the western coastlines (Namibia and Angola) contrasting with intense precipitation along the eastern coastlines of South Africa, a phenomenon linked to the triple-dip La Niña conditions (Thoithi *et al* 2026).

Figure 1(c) presents the probability density function (PDF) and the histogram of raw Rx1d values. While a normal distribution fails to adequately capture the spread and tail behavior of the data, the GEV distribution fitted to the 30 year base period (1985–2014) provides a reasonable fit. We verified the validity of using this 30 year baseline by comparing it with the 74 year (1950–2023) GEV fit; both distributions remain within each other's 90% uncertainty intervals, and the resulting risk estimates for the 2023 event are nearly identical (e.g. 0.65% vs. 0.68% for the 1st-rank event). Consequently, we focus on the GEV derived from the 1985–2014 period to minimize the influence of transient global warming trends on our baseline estimates (Abdelmoaty and Papalexiou 2023).

To assess the relationship between extreme event frequency and intensity, figure 1(d) shows the return level plot. The return levels derived from the 74 and 30 year GEV distributions are consistent and well within the 90% confidence ranges, further confirming the robustness of the 30 year baseline for estimating Rx1d risks. In this study, we define three specific return periods for further analysis: 150, 70, and 10 year events, which match the magnitude of the 1st-highest (2023), 2nd-highest (2000), and a typical decadal extreme, respectively. It should be noted that the 70 and 150 year thresholds are extrapolated from stationary GEV fits to the 30 year reference

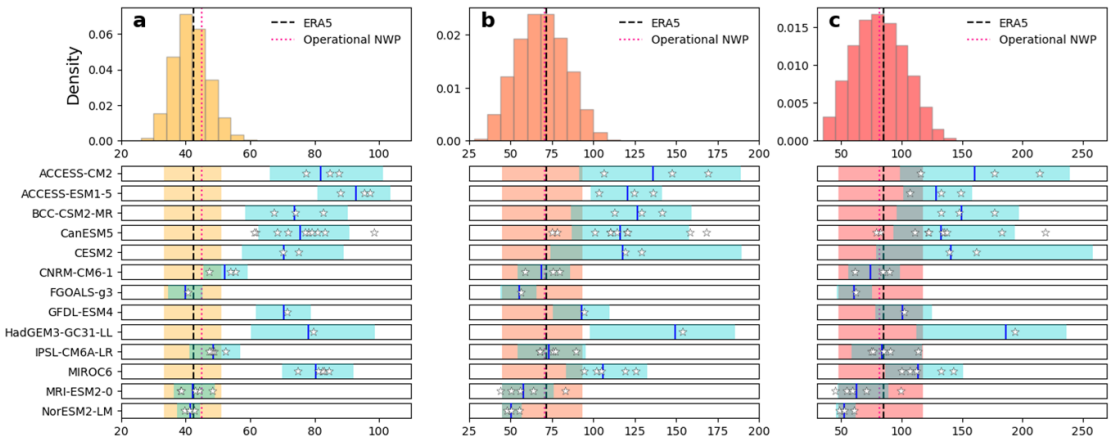


Figure 2. Distributions of ERA5 Rx1d intensity for (a) 10-year (orange), (b) 70-year (peach), and (c) 150-year (red) return periods, derived from bootstrapped GEV resamples of the base period. Dashed and dotted lines represent the GEV estimates for ERA5 and the operational NWP (1985–2014) without bootstrapping, respectively. For comparison, corresponding results from 13 CMIP6 ESMs are shown, displaying individual ensemble members (asterisks), bootstrapped medians (blue marks), and 90% confidence intervals (turquoise shading).

period and are not presented as observed recurrence intervals.

3.2. Extreme events evaluation for models

Since both MPA and SPA rely on simulated output, we evaluate the performance of ESMs and NWP in replicating the target extreme events (figure 2). The bar graphs represent the bootstrapped GEV results from ERA5, illustrating the 90% confidence intervals for extreme event magnitude at specific return periods (10, 70, and 150 years; figure 1(d)). The return values for operational NWP closely align with ERA5, with GEV parameters (μ, σ, ξ) falling within the ERA5 uncertainty ranges (supplementary figure 2).

In contrast, the 13 ESMs and their respective ensembles (supplementary table 2) exhibit a wide spread in return values, reflecting differences in model physics, dynamics, and internal climate variability (figure 2; supplementary figure 2). Notably, most ESMs exhibit a significant wet bias in the 10 year extreme values, where the 90% uncertainty ranges of the ESMs and ERA5 do not overlap (figure 2(a)). While this wet bias persists for the 70 year and 150 year return levels, it is less pronounced than in the 10 year case (figures 2(b) and (c)).

GEV parameter analysis reveals that this wet bias originates primarily from positive biases in μ and σ, indicating an overestimation of the climatological mean and interannual variability of Rx1d (supplementary figure 2). In contrast, ξ for most ESMs remains within the ERA5 uncertainty range. Although μ and σ across the 13 ESMs are highly correlated ($r = 0.81$, supplementary table 4), substantial inter-model and inter-ensemble spread remains. Given these bias characteristics, we present ESM results primarily as anomalies to mitigate systematic errors (figures 3(a) and 4(a)), while NWP results are presented as absolute values (figures 3(b) and 4(b)).

3.3. Extreme events attribution

We examine NWP and ESM simulations under varying forcing conditions to attribute changes in extreme event risks (figure 3). The pooled-median PDF of the 13 ESMs' bootstrapped resamples (figure 3(a)) demonstrates that GHG forcing induces the most pronounced change in the distribution: the tail for severe extreme rainfall becomes significantly heavier, while the density near the climatological mean decreases. Probabilities of extreme events in AER simulations are lower than those in ALL-forcing simulations. Notably, the ALL (factual) results closely mirror the combined signals of GHG and AER, confirming their opposing influences on Rx1d.

Our main NWP-S group and the sensitivity tests (NWP-M and NWP-L) consistently indicate that CO_2-driven ocean warming and increased radiative forcing elevate the probability of 2023-like extremes (figure 3(b); ALL vs. PIC). This aligns with the broader ESM results (ALL/GHG vs. NAT). The PDF of short-range predictions (NWP-S) aligns closely with the observed 2023 magnitude, whereas long-range predictions (NWP-L) shift toward the climatological mean, illustrating how synoptic predictability constrains the simulation of observed weather systems.

The median RR from the 13 ESMs exceed one across nearly all targets (figure 3(c)). Consistent with the PDF shifts (figure 3(a)), GHG-forced risk increases are 'likely' (>66 confidence) for all targets, with GHG simulations showing the smallest uncertainty and AER the largest. This AER-driven uncertainty likely explains past TPA inconsistencies (Fučkar *et al* 2020, Otto *et al* 2022, Pinto *et al* 2026). Furthermore, we demonstrate 'likely' significance for

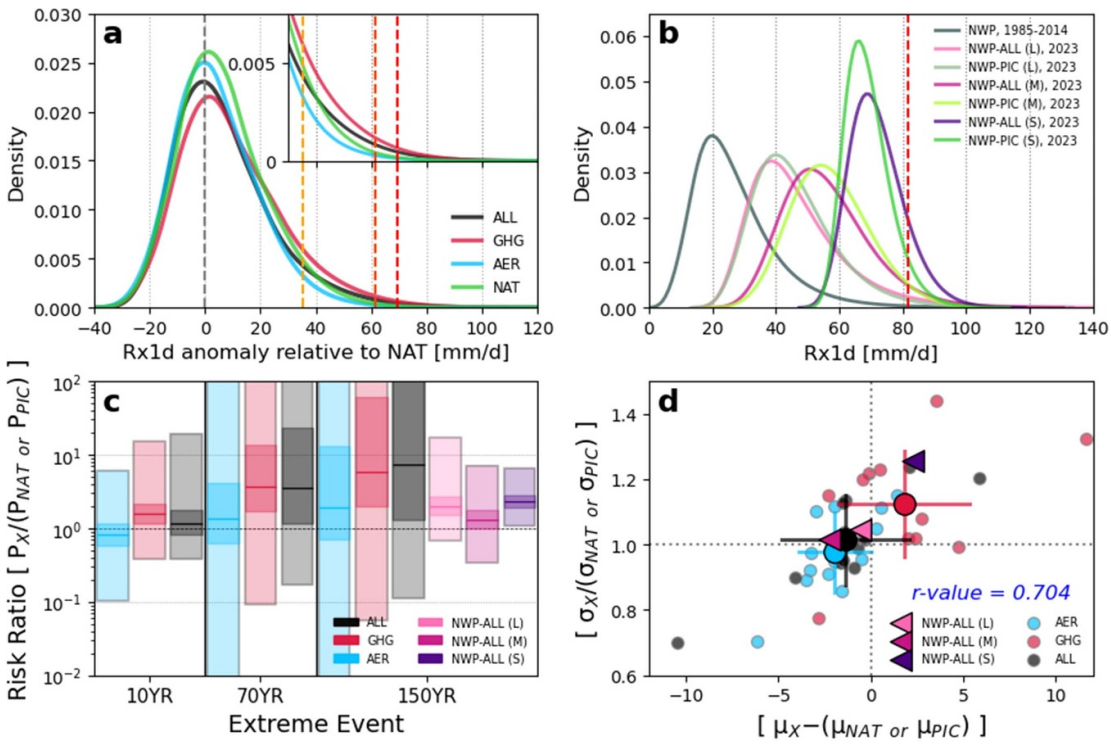


Figure 3. (a) Pooled-median probability density functions (PDFs) of bootstrapped resamples (1 300 000) of Rx1d anomalies for the 13 ESMs under ALL, GHG, AER, and NAT forcings, calculated relative to μ of each NAT simulation. Dashed lines highlight the pooled-median anomaly return levels for 10-year (yellow), 70-year (orange), and 150-year (red) events, with the inset showing a magnified view of the distribution tails. (b) Bootstrapped-median Rx1d PDFs for NWP-S, NWP-M, and NWP-L under ALL and PIC forcing conditions designed for the 2023 event, with the operational NWP baseline included for comparison. (c) Risk Ratio (RR) under ALL, GHG, and AER forcings for the target 10-, 70-, and 150-year extreme events. Light and dark shaded bars denote the 5%–95% and 34%–66% uncertainty ranges, respectively, indicating the significance of RR changes. Solid horizontal lines mark the median values of ESMs' pooled bootstrapped resamples. NWP results are shown only for the 150-year event due to experimental design constraints. (d) Scatter plot of differences in μ (abscissa) versus changes in σ (ordinate), for the ESMs and NWP relative to their parameters in NAT and PIC. Small and large dots represent individual models and their mean values, respectively, with error bars (solid lines) indicating one standard deviation across the 13 ESMs. The correlation coefficient (blue text) is significant at the 5% level.

severe events (70-year and 150 year), which were inconclusive in prior TPA studies. This highlights the importance of accounting for non-linearity in EEA, as our MPA framework utilizes dynamically integrated simulations. Notably, NWP-S results show 'extremely likely' (>95% confidence) significance, due to tighter constraints on synoptic evolution and ocean variability.

Figure 3(d) examines GEV parameters, showing higher μ and σ under GHG-forced ESMs and NWP-ALL (S) compared to NAT/PIC, confirming them as drivers of increased risks. Their robust correlation reaffirms the coupling between climatological means and interannual variability, as previously identified in ESM bias characteristics (supplementary figure 2; supplementary table 4). Conversely, ESM-ALL parameters closely resemble NAT, unlike the clear differences in NWP-ALL (S) versus NWP-PIC (S). This stems from: (1) ESM experiments include AER forcing, which partially offsets GHG impact via thermodynamical and potentially dynamical effects (Huang *et al* 2023, Wang *et al* 2026), whereas NWP experiments focus solely on CO_2 and associated warmings. (2) ESM ensemble diversity in ocean variability hinders the clear direct forcing-driven impact, unlike the NWP experiments with almost identical ocean states (supplementary figure 3). Finally, while ξ changes remain statistically insignificant due to high uncertainty, some RR results are only explainable when considering changes in ξ. The broader implications of AER, ocean variability and ξ are addressed in section 4.

3.4. Extreme events projections

To address the potential benefits of global warming mitigation, we examine future changes in extreme rainfall under various projection scenarios, differing mainly in GHG mitigation level (figure 4). The PDF shifts in ESM projections relative to current conditions (ALL) mirror the changes observed in GHG-forced simulations compared to natural forcings (figure 3(a)): the probability of climatological mean-like Rx1d decreases, while the density of high-magnitude extreme events increases (figure 4(a)). Notably, the lowest-emission scenario (SSP1-2.6) exhibits the least modification, whereas

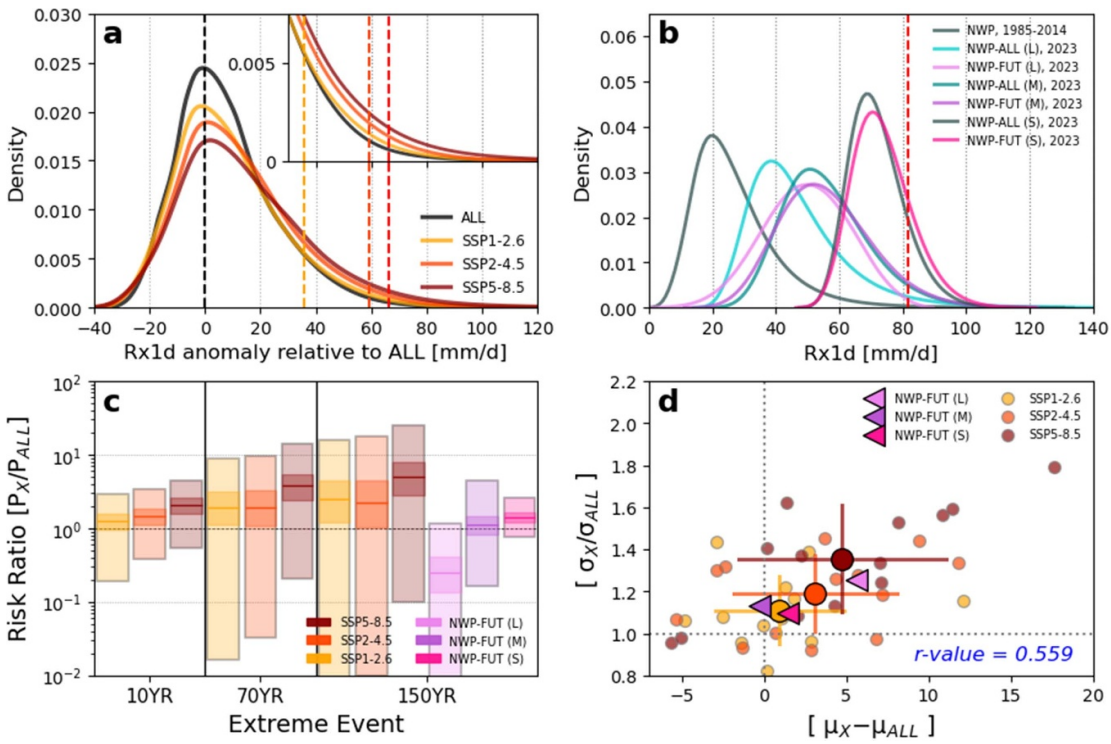


Figure 4. (a) Pooled-median probability density functions (PDFs) of bootstrapped resamples (1 300 000) of Rx1d anomalies for the 13 ESMs under the SSP1-2.6, SSP2-4.5, and SSP5-8.5 future scenarios. Dashed lines highlight the pooled-median anomaly return levels for 10-year (yellow), 70-year (orange), and 150-year (red) events, with the inset showing a magnified view of the distribution tails. (b) Bootstrapped-median Rx1d PDFs for NWP-S, NWP-M, and NWP-L under the ALL and FUT forcing conditions designed for the 2023 event, with the operational NWP baseline included for comparison. (c) Risk Ratio (RR) under the SSP scenarios for the target 10-, 70-, and 150-year extreme events. Light and dark shaded bars denote the 5%–95% and 34%–66% uncertainty ranges, respectively. Solid horizontal lines mark the median values of ESMs' pooled bootstrapped resamples. NWP results are shown only for the 150-year event due to experimental design constraints. (d) Scatter plot of differences in μ (abscissa) versus changes in σ (ordinate), for the ESMs and NWP relative to their parameters in ALL. Small and large dots represent individual models and their mean values, respectively, with error bars (solid lines) indicating one standard deviation across the 13 ESMs. The correlation coefficient (blue text) is significant at the 5% level.

high-emission scenarios (SSP5-8.5) lead to substantial transformation, underscoring the necessity of mitigation to minimize future Rx1d distribution shifts.

NWP-FUT simulations, while similar to the SSP2-4.5 (with invariant non-CO_2 forcings), show PDF shifts relative to NWP-ALL (figure 4(b)) consistent with those of NWP-ALL versus NWP-PIC attribution (figure 3(b)). Since NWP-L shows the broadest distributions and lowest predictability due to chaotic weather noise (supplementary figure 1), it is less suitable for the storyline framework; thus, we prioritize the NWP-S for robust projections.

Relative to ESMs' ALL, projected RR for target extreme events increases are classified as 'likely' across most scenarios, except for 10 year events under SSP1-2.6 (figure 4(c)). These projections align with our GHG attribution findings (figure 3(c)), indicating that even under the most stringent mitigation (SSP1-2.6), the risk of high-impact events (70 and 150 year) remains elevated. Nevertheless, aggressive mitigation is essential, as the magnitude of RR significantly increases with warming (SSP2-4.5 and SSP5-8.5). In NWP-FUT (S), the RR for 2023-like events (150-year) is projected to increase ('likely'), consistent with ESM findings. An unexpected finding in NWP-L is the projected decrease in RR for specific cases, despite expansions in μ and σ. This suggests that occasionally, changes in ξ may determine the risk assessment, an effect often unconsidered by simpler linear statistical methods (figures 4(b) and (d); supplementary table 4).

Finally, we assess the impact of GHG mitigation scenarios on GEV parameters (figure 4(d)). Increased radiative forcing under SSP and NWP-FUT scenarios leads to higher μ and σ values, consistent with our attribution results (figure 3(d)). A crucial observation is that for ESMs, the projected shifts in σ under SSP5-8.5 and SSP2-4.5 exceed inter-model spread (noise), yielding a signal-to-noise ratio (S/N >1; Lee *et al* 2024), which confirms the statistical significance of these shifts. All three NWP lead-time groups consistently indicate positive shifts in these parameters. Consequently, these results highlight that strict GHG regulation is critical as only the lowest scenario (SSP1-2.6) suggests an insignificant shift in GEV parameters, implying a potential to stabilize the Rx1d distribution in the SEAF region.

4. Summary and discussion

Extreme rainfall in SEAF reached record-breaking levels in 2023 (Fazel-Rastgar *et al* 2025). Determining anthropogenic contributions remains challenging due to discrepancies between observational trends and climate models (Pinto *et al* 2026). To address these uncertainties, this study employs both MPA and SPA. By synthesizing these methods, we reconcile inconsistencies found in previous TPA studies (Otto *et al* 2022, Pinto *et al* 2026). We further quantify projected risk changes under various global warming scenarios, underscoring the critical necessity of mitigation.

Observational analysis confirms the 2000 and 2023 events were highly anomalous (Jury and Lucio 2004, Fazel-Rastgar *et al* 2025). Both shared identical climate drivers: La Niña conditions and pronounced positive Sea Surface Temperature (SST) anomalies in the South-West Indian Ocean (Thoithi *et al* 2026). La Niña phases enhance large-scale moisture fluxes toward southeastern Africa and promote unusually long, zonal cyclone tracks (Richard *et al* 2000). Furthermore, anomalously warm SST in the Mozambique Channel provided an immense latent heat reservoir, allowing tropical cyclones to intensify before landfall and resulting in devastating extremes like Eline (Reason and Keibel 2004) and Freddy (Liu *et al* 2023).

While station-based datasets exhibit spatio-temporal limitations, ERA5 reanalysis provides robust frequency and magnitude metrics. Our NWP experiments successfully replicate these extreme records, whereas most ESMs exhibit a systematic wet bias stemming from overestimations in the μ and σ parameters (figure 2; supplementary figure 2). This necessitates using relative thresholds for ESM analysis. Reducing these biases through improved parameterization remains critical for enhancing ESM credibility (e.g. Lee *et al* 2022a, Schaffer *et al* 2025, Seo *et al* 2025). Notably, applying spatial interpolation or subsampling the best performing ESMs yielded insignificant difference in our results (supplementary Text 2 and supplementary figures 4 and 5).

Despite these inter-model variations, there is strong consensus that GHG forcing increases the mean and interannual variability of extreme rainfall, whereas AER plays an opposing, albeit more uncertain, role (Samset *et al* 2018, Westervelt *et al* 2020, Li *et al* 2023, Wang *et al* 2026). Thermodynamically, GHG amplify extremes by increasing tropospheric moisture capacity, which is directly offset by AER cooling (O'Gorman 2015, Huang *et al* 2023). Dynamically, GHG modify convective updrafts, while localized AER emissions distort regional temperature gradients and major circulation patterns like the ITCZ (Persad and Caldeira 2018, Sheng *et al* 2026).

Our projections confirm high-emission pathways (SSP5-8.5) yield higher risks than sustainable scenarios (SSP1-2.6). Since GHG is the primary forcing difference across SSPs (Riahi *et al* 2017), these mitigation benefits mirror our attribution findings. Our NWP-S results align with these ESM projections, supporting the interpretation of CO_2-driven radiative forcing and SST warming as primary drivers. Meanwhile, NWP sensitivity tests (NWP-M & NWP-L) show this forcing signal degrades as predictability decreases. Despite atmospheric adjustment caveats (supplementary Text 3 and supplementary figures 6 and 7), GHG remains the dominant driver, making aggressive mitigation essential to prevent extreme event distribution shifts (Lee *et al* 2018, Ayugi *et al* 2023, Bobde *et al* 2024, Seo *et al* 2025). Although primarily GHG-driven, ESM projections encompass combined non-GHG effects.

NWP results exhibit lower uncertainty than ESMs, due to the constraint of synoptic weather systems (e.g. Leach *et al* 2024, Lee *et al* 2024) and consistent ocean states (e.g. Deser *et al* 2020, Lee *et al* 2022b). While eastern Pacific SST variability influences SEAF Rx1d (Richard *et al* 2000, Tadross 2009, Pinto *et al* 2026, Thoithi *et al* 2026), we find that inter-model spread is strongly associated with the southern Indian Ocean temperature contrast (supplementary figures 3(c) and (d)). This regional gradient is linked to the intensification of landfalling extreme weather systems (Reason and Keibel 2004, Liu *et al* 2023). Furthermore, as global warming can enhance cross-basin teleconnections (e.g. Chen *et al* 2026), the emerging impacts of varying SST patterns on SEAF Rx1d represent an important topic for future study.

Previous TPA studies struggled to detect significant attribution signals from factual ALL-forcing simulations (Otto *et al* 2022, Pinto *et al* 2026). Our MPA results elucidate that while GHG 'likely' increases extreme events risks, high uncertainty in AER-driven responses masks this signal in ALL-forcing simulations. Consequently, linearly varying GEV parameters in TPA may underestimate forcing-driven nonlinearity. By synthesizing MPA and SPA, we robustly conclude that GHG and CO_2 forcings significantly elevate extreme event risks. Without substantial mitigation, our projections indicate SEAF will continue to face elevated extreme rainfall risks, a conclusion further supported by our model-by-model analysis (supplementary figures 8 & 9).

Finally, we confirm a forcing-driven relationship between GEV parameters (μ & σ). While traditional TPA assumes a constant ξ (e.g. Salas and Obeysekera 2014), we highlight its high sensitivity and variance. We note that the comparison of stationary GEV fits across different experiments is not equivalent to a formal nonstationary GEV analysis. In our current framework, apparent differences in ξ are heavily obscured by high estimation uncertainty,

preventing the confident detection of robust physical shifts. Consequently, we observed no significant ESM-averaged changes in ξ. To overcome such statistical limitations, future research focusing on the physical interpretation of tail behaviour (ξ) is required to further refine EEA and projection frameworks (e.g. Jayaweera *et al* 2025).

Acknowledgments

We acknowledge the World Climate Research Programme, which, through its Working Group on Coupled Modelling, coordinated and promoted CMIP6. We acknowledge the climate modeling groups for producing and making available their model output, the Earth System Grid Federation (ESGF) for archiving the data and providing access, and the multiple funding agencies who support CMIP6 and ESGF. This work used JASMIN, the UK collaborative data analysis facility. Acknowledgement is made for the use of ECMWF's computing and archive facilities in this research under the special project spgbleac. We also thank the Department of Physics at Imperial College London for supporting Carol Chen's participation in this research through the Undergraduate Research Opportunities Programme (UROP) Project 2025. We also acknowledge support by UK Research and Innovation (UKRI) under the UK government's Horizon Europe funding Guarantee, Grant EP/Y036123/1 (P.C.), and by UKRI Natural Environment Research Council (NERC) Grants NE/T006250/1 (D.L. and P.C.). Finally, we would like to thank the anonymous reviewers for their time and feedback. In particular, we are deeply grateful for the constructive and insightful comments that significantly refined our methodological approach and strengthened the overall clarity and robustness of this research.

Data availability statement

The CMIP6 model data sets that support the findings of this study are openly available at: https://esgf-node.llnl.gov/projects/cmip6/. All NWP experimental data used in this study are available via the ECMWF MARS archive (www.ecmwf.int/en/forecasts/datasets) under experiment IDs b2r0, b2r1, b2r7, b2r8, and b2r9, subject to access permission. Detailed information can be found at https://apps.ecmwf.int/ifs-experiments/uk/b2r7.

Supplementary data 1 available at: https://doi.org/10.1088/1748-9326/aea7b9/data1.

Code Availability

The code used for data processing, statistical analysis, and figure generation is available from the corresponding author upon reasonable request.

Author contributions

Donghyun Lee 0000-0003-0184-2712
Conceptualization (lead), Data curation (lead), Investigation (lead), Methodology (lead), Supervision (lead), Validation (lead), Visualization (lead), Writing – original draft (lead), Writing – review & editing (equal)

Carol Chen 0009-0004-3084-0665
Data curation (supporting), Formal analysis (lead), Investigation (equal), Visualization (equal), Writing – original draft (equal)

Paulo Ceppi 0000-0002-3754-3506
Funding acquisition (lead), Investigation (equal), Project administration (lead), Supervision (equal), Visualization (equal), Writing – review & editing (equal)

Friederike Otto 0000-0001-8166-5917
Investigation (equal), Methodology (equal), Writing – review & editing (equal)

In-Hong Park 0000-0001-7222-8168
Methodology (equal), Validation (equal), Visualization (equal), Writing – review & editing (equal)

Nicholas Leach 0000-0003-4470-1813
Investigation (equal), Resources (lead), Validation (equal), Writing – review & editing (equal)

Sarah Sparrow 0000-0002-1802-6909
Data curation (supporting), Resources (equal), Writing – review & editing (equal)

Myles Allen 0000-0002-1721-7172
Conceptualization (equal), Resources (equal), Writing – review & editing (equal)

References

Abdelmoaty H M and Papalexiou S M 2023 Changes of extreme precipitation in CMIP6 projections: should we use stationary or nonstationary models? *J. Clim.* **36** 2999–3014

Aderinto N 2023 Tropical Cyclone Freddy exposes major health risks in the hardest-hit Southern African countries: lessons for climate change adaptation *Int. J. Surg. Glob. Health* **6** e0152

Allen M 2003 Liability for climate change *Nature* **421** 891–2

Ayugi B O, Chung E S, Zhu H, Ogega O M, Babousmail H and Ongoma V 2023 Projected changes in extreme climate events

over Africa under 1.5° C, 2.0° C and 3.0° C global warming levels based on CMIP6 projections *Atmos. Res.* **292** 106872
Banda S and Bangidza L B 2025 The impact of tropical cyclones on human security: a case of mozambique and Zimbabwe (2000–2019) *Disaster Risks and Hazards: Practice for Resilience-Case for Zimbabwe* (Springer) pp 205–33
Barriopedro D, Jiménez-esteve B, Collazo S, Garrido-perez J M, Johnson J E and García-herrera R 2025 A multimethod attribution analysis of Spain's 2024 extreme precipitation event *Bull. Am. Meteorol. Soc.* **106** E2440–E60
Becker A, Finger P, Meyer-christoffer A, Rudolf B, Schamm K, Schneider U and Ziese M 2013 A description of the global land-surface precipitation data products of the global precipitation climatology centre with sample applications including centennial (trend) analysis from 1901–present *Earth Syst. Sci. Data* **5** 71–99
Bobde V, Akinsanola A A, Folorunsho A H, Adebiyi A A and Adeyeri O E 2024 Projected regional changes in mean and extreme precipitation over Africa in CMIP6 models *Environ. Res. Lett.* **19** 074009
Braka F, Daniel E O, Okeibunor J, Rusibamayila N K, Conteh I N, Ramadan O P C and Gueye A S 2024 Effects of tropical cyclone Freddy on the social determinants of health: the narrative review of the experience in Malawi *BMJ Public Health* **2** e000512
Chen S, Chen W, Wu R, Xie S P, Wang C, Yeh S W and Song L 2026 Enhanced influence of tropical Atlantic variability on East Asian summer monsoon in warming climate *Innov. Geosci.* **4** 100207–1
Davison A C and Hinkley D V 1997 *Bootstrap Methods and Their Application (No. 1)* (Cambridge University Press)
Deser C, Lehner F, Rodgers K B, Ault T, Delworth T L, DiNezio P N and Ting M 2020 Insights from Earth system model initial-condition large ensembles and future prospects *Nat. Clim. Change* **10** 277–86
Dong S, Sun Y, Li C, Zhang X, Min S K and Kim Y H 2021 Attribution of extreme precipitation with updated observations and CMIP6 simulations *J. Clim.* **34** 871–81
Dunn R J, Herold N, Alexander L V, Donat M G, Allan R, Bador M and Zhang X 2024 Observed global changes in sector-relevant climate extremes indices—an extension to HadEX3 *Earth Space Sci.* **11** e2023EA003279
ECMWF 2021 *IFS Documentation CY47R3—Part V: ensemble prediction system* (European Centre for Medium-Range Weather Forecasts) (https://doi.org/10.21957/zw5j5zdz5)
Ermis S, Leach N J, Lott F C, Sparrow S N and Weisheimer A 2024 Event attribution of a midlatitude windstorm using ensemble weather forecasts *Environ. Res. Clim.* **3** 035001
Eyring V, Bony S, Meehl G A, Senior C A, Stevens B, Stouffer R J and Taylor K E 2016 Overview of the Coupled Model Intercomparison Project Phase 6 (CMIP6) experimental design and organization *Geosci. Model Dev.* **9** 1937–58
Fazel-Rastgar F, Sivakumar V, Rostami M and Fallah B 2025 Unveiling meteorological synergies in the coupling of an abnormal easterly wave and cutoff low in South Africa's February 2023 rainfall *Meteorol. Appl.* **32** e70027
Forbes R, Laloyaux P and Rodwell M 2021 IFS upgrade improves moist physics and use of satellite observations *ECMWF Newsl.* **169** 13–22
Fučkar N S, Otto F E, Lehner F, Pinto I, Howard E, Sparrow S and Wallom D 2020 On high precipitation in Mozambique, Zimbabwe, And Zambia In February 2018 *Bull. Am. Meteorol. Soc.* **101** S47–S52
Gillett N P, Shiogama H, Funke B, Hegerl G, Knutti R, Matthes K and Tebaldi C 2016 The detection and attribution model intercomparison project (DAMIP v1. 0) contribution to CMIP6 *Geosci. Model Dev.* **9** 3685–97
Haustein K, Otto F E L, Uhe P, Schaller N R A M, Allen M R, Hermanson L and Cullen H 2016 Real-time extreme weather event attribution with forecast seasonal SSTs *Environ. Res. Lett.* **11** 064006
Hersbach H, Bell B, Berrisford P, Hirahara S, Horányi A, Muñoz-sabater J and Thépaut J N 2020 The ERA5 global reanalysis *Q. J. R. Meteorol. Soc.* **146** 1999–2049
Huang Z, Tan X, Gan T Y, Liu B and Chen X 2023 Thermodynamically enhanced precipitation extremes due to counterbalancing influences of anthropogenic greenhouse gases and aerosols *Nat. Water* **1** 614–25
Huffman G J, Adler R F, Behrangi A, Bolvin D T, Nelkin E J, Gu G and Ehsani M R 2023 The new version 3.2 Global Precipitation Climatology Project (GPCP) monthly and daily precipitation products *J. Clim.* **36** 7635–55
Jayaweera L, Wasko C and Nathan R 2025 Evidence for non-stationarity in the GEV shape parameter when modeling extreme rainfall *Water Resour. Res.* **61** e2023WR036426
Jury M R and Lucio F D E 2004 The Mozambique floods of February 2000 in context *South. Afr. Geogr. J.* **86** 141–6
Kause A, Bruine de Bruin W, Persson J, Thorén H, Olsson L, Wallin A and Vareman N 2022 Confidence levels and likelihood terms in IPCC reports: a survey of experts from different scientific disciplines *Clim. Change* **173** 2
Kharin V V, Zwiers F W, Zhang X and Hegerl G C 2007 Changes in temperature and precipitation extremes in the IPCC ensemble of global coupled model simulations *J. Clim.* **20** 1419–44
Kim Y H, Lee M, Min S K, Park D S R, Cha D H, Byun Y H and Heo J 2024 Global warming–induced warmer surface water over the East China Sea can intensify typhoons like Hinnamnor *Bull. Am. Meteorol. Soc.* **105** E1416–E21
Kim Y H, Min S K, Zhang X, Sillmann J and Sandstad M 2020 Evaluation of the CMIP6 multi-model ensemble for climate extreme indices *Weather Clim. Extrem.* **29** 100269
Kodra E and Ganguly A R 2014 Asymmetry of projected increases in extreme temperature distributions *Sci. Rep.* **4** 5884
Leach N J, Roberts C D, Aengenheyster M, Heathcote D, Mitchell D M, Thompson V and Allen M R 2024 Heatwave attribution based on reliable operational weather forecasts *Nat. Commun.* **15** 4530
Leach N J, Weisheimer A, Allen M R and Palmer T 2021 Forecast-based attribution of a winter heatwave within the limit of predictability *Proc. Natl Acad. Sci. USA* **118** e2112087118
Lee D, Min S K, Fischer E, Shiogama H, Bethke I, Lierhammer L and Scinocca J F 2018 Impacts of half a degree additional warming on the Asian summer monsoon rainfall characteristics *Environ. Res. Lett.* **13** 044033
Lee D, Min S K, Park I H, Ahn J B, Cha D H, Chang E C and Byun Y H 2022a Enhanced role of convection in future hourly rainfall extremes over South Korea *Geophys. Res. Lett.* **49** e2022GL099727
Lee D, Sparrow S, Leach N, Osprey S, Lee J and Allen M 2024 The attribution of February extremes over North America: a forecast-based storyline study *J. Clim.* **37** 5073–89
Lee S, L'heureux M, Wittenberg A T, Seager R, O'Gorman P A and Johnson N C 2022b On the future zonal contrasts of equatorial Pacific climate: perspectives from observations, simulations, and theories *npj Clim. Atmos. Sci.* **5** 82
León-FonFay D, Lemburg A, Fink A H, Pinto J G and Feser F 2026 A combined storyline-statistical approach for conditional extreme event attribution *Weather Clim. Dynam.* **7** 597–613
Li R, Liu X, Xu Y and Dong B 2023 A comparative analysis of the attribution of extreme summer precipitation in south and north parts of the East China monsoon region—with the year 2020 as an example *Int. J. Climatol.* **43** 7199–217
Liu H Y, Satoh M, Gu J F, Lei L, Tang J, Tan Z M and Xu J 2023 Predictability of the most long-lived tropical cyclone Freddy (2023) during its westward journey through the southern tropical Indian Ocean *Geophys. Res. Lett.* **50** e2023GL105729
Malardel S, Wedi N, Deconinck W, Diamantakis M, Kühnlein C, Mozdzynski G and Smolarkiewicz P 2016 A new grid for the IFS *ECMWF Newsl.* **146** 23–28 (available at: https://www.ecmwf.int/sites/default/files/elibrary/2016/17262-new-grid-ifs.pdf)

Mastrandrea M D, Mach K J, Plattner G K, Edenhofer O, Stocker T F, Field C B and Matschoss P R 2011 The IPCC AR5 guidance note on consistent treatment of uncertainties: a common approach across the working groups *Clim. Change* **108** 675

Min S K 2020 Human fingerprint in global weather *Nat. Clim. Change* **10** 15–16

Min S K, Zhang X, Zwiers F W, Friederichs P and Hense A 2009 Signal detectability in extreme precipitation changes assessed from twentieth century climate simulations *Clim. Dyn.* **32** 95–111

Nganhane H V, Tavares A O, Santos P P and Fernández-sánchez A 2025 Tropical cyclone meteorological extreme events and their large impacts in Mozambique during the period 1926–2021 *Comun. Geol.* **112** 267–71

Nordling K, Fahrenbach N L and Samset B H 2025 Climate variability can outweigh the influence of climate mean changes for extreme precipitation under global warming *Atmos. Chem. Phys.* **25** 1659–84

O'Gorman P A 2015 Precipitation extremes under climate change *Curr. Clim. Change Rep.* **1** 49–59

Otto F E, Zachariah M, Wolski P, Pinto I, Nhamtumbo B, Bonnet R and Harrington L J 2022 Climate change increased rainfall associated with tropical cyclones hitting highly vulnerable communities in Madagascar, Mozambique & Malawi *Mozambique & Malawi* p 41

Perkins-Kirkpatrick S E, Stone D A, Mitchell D M, Rosier S, King A D, Lo Y T E and Wehner M 2022 On the attribution of the impacts of extreme weather events to anthropogenic climate change *Environ. Res. Lett.* **17** 024009

Persad G G and Caldeira K 2018 Divergent global-scale temperature effects from identical aerosols emitted in different regions *Nat. Commun.* **9** 3289

Philip S, Kew S, van Oldenborgh G J, Otto F, Vautard R, van Der Wiel K and van Aalst M 2020 A protocol for probabilistic extreme event attribution analyses *Adv. Stat. Climatol. Meteorol. Oceanogr.* **6** 177–203

Pinto I *et al* 2026 *La Niña, Climate Change, High Exposure and Vulnerability Combined Led to Devastating Floods in Parts of Southern Africa* (World Weather Attribution) (WWA scientific report No. 81) (https://doi.org/10.25560/127388)

Reason C J C and Keibel A 2004 Tropical cyclone Eline and its unusual penetration and impacts over the southern African mainland *Weather Forecast.* **19** 789–805

Riahi K, Van Vuuren D P, Kriegler E, Edmonds J, O'neill B C, Fujimori S and Tavoni M 2017 The shared socioeconomic pathways and their energy, land use, and greenhouse gas emissions implications: an overview *Glob. Environ. Change* **42** 153–68

Richard Y, Trzaska S, Roucou P and Rouault M 2000 Modification of the southern African rainfall variability/ENSO relationship since the late 1960s *Climate Dynamics* **16** 883–95

Salas J D and Obeysekera J 2014 Revisiting the concepts of return period and risk for nonstationary hydrologic extreme events *J. Hydrol. Eng.* **19** 554–68

Samset B H, Sand M, Smith C J, Bauer S E, Forster P M, Fuglestvedt J S and Schleussner C F 2018 Climate impacts from a removal of anthropogenic aerosol emissions *Geophys. Res. Lett.* **45** 1020–9

Schaffer A, Lichtenegger T, Ossó A and Maraun D 2025 Resolution dependence and biases in cold and warm frontal heavy precipitation over Europe in CMIP6 and EURO-CORDEX models *Weather Clim. Dyn.* **6** 1815–30

Seo G Y, Min S K, Lee D, Son S W, Park C and Cha D H 2025 Hourly extreme rainfall projections over South Korea using convection permitting climate simulations *npj Clim. Atmos. Sci.* **8** 209

Serele C, Kouadio M and Kayitakire F 2023 Mitigating proximate impacts of tropical cyclone landfalls in the Southwest Indian Ocean *West. Indian Ocean J. Mar. Sci.* **22** 147–61

Sheng B, Bollasina M A, Gagnon A S, Wilcox L J, Reynolds T P, Beckett C T and Koshiro T 2026 East Asian anthropogenic aerosols strongly influence past and present Southern African hydroclimate and ecosystem changes *EGUsphere* **2026** 1–25

Shepherd T G, Boyd E, Calel R A, Chapman S C, Dessai S, Dima-west I M and Zenghelis D A 2018 Storylines: an alternative approach to representing uncertainty in physical aspects of climate change *Clim. Change* **151** 555–71

Sillmann J, Kharin V V, Zhang X, Zwiers F W and Bronaugh D 2013 Climate extremes indices in the CMIP5 multimodel ensemble: part 1. Model evaluation in the present climate *J. Geophys. Res. Atmos.* **118** 1716–33

Tadross M 2009 Climate change modelling and analyses for Mozambique *Report prepared for Instituto Nacional de Gestão de Calamidades* (https://doi.org/10.1111/j.1365-2818.2008.03109.x)

Takahashi C, Imada Y, Kawase H and Tanaka T 2025 A new statistical method of rapid event attribution for probability of extreme events: applications to heatwave events in Japan *Environ. Res. Clim.* **4** 035001

Taylor R G, Todd M C, Kongola L, Maurice L, Nahozya E, Sanga H and MacDonald A M 2013 Evidence of the dependence of groundwater resources on extreme rainfall in East Africa *Nat. Clim. Change* **3** 374–8

Thoithi W, Blamey R C and Reason C J 2026 Circulation anomalies associated with mid-to late summer rainfall differences during multiyear La Niña events over subtropical southeastern Africa *Clim. Dyn.* **64** 128

Van Garderen L, Feser F and Shepherd T G 2021 A methodology for attributing the role of climate change in extreme events: a global spectrally nudged storyline *Nat. Hazards Earth Syst. Sci.* **21** 171–86

Wang L, Chen S, Chen W, Cai Q, Ma T, Zheng Y and Song L 2026 Recent accelerated drying in southwest China dominated by anthropogenic aerosol forcing *Environ. Res. Lett.* **21** 014035

Wang L, Gu X, Slater L J, Lai Y, Zheng Y, Gong J and Li J 2023 Attribution of the record-breaking extreme precipitation events in July 2021 over central and eastern China to anthropogenic climate change *Earth Future* **11** e2023EF003613

Wehrli K, Hauser M and Seneviratne S I 2020 Storylines of the 2018 Northern Hemisphere heatwave at pre-industrial and higher global warming levels *Earth Syst. Dyn.* **11** 855–73

Westervelt D M, You Y, Li X, Ting M, Lee D E and Ming Y 2020 Relative importance of greenhouse gases, sulfate, organic carbon, and black carbon aerosol for South Asian monsoon rainfall changes *Geophys. Res. Lett.* **47** e2020GL088363